Normalized Hail Particle Size Distributions from the T-28 Storm Penetrating Aircraft

Paul R. Field[1,2], Andrew J. Heymsfield[3], Andrew G. Detwiler[4] and Jonathan M. Wilkinson[1]

1 Met Office, Exeter, UK

2 ICAS Univ. of Leeds, Leeds, UK

3 NCAR, Boulder, CO, USA.

4 Department of Physics, and Atmospheric and Environmental Sciences Program, SDSM&T, Rapid City, SD, USA.

Corresponding author: Paul Field (paul.field@metoffice.gov.uk)

Abstract

Hail and graupel are linked to lightning production and are important components of cloud evolution. Hail can also cause significant damage when it precipitates to the surface. The accurate prediction of the amount and location of hail and graupel and the effects on the other hydrometeor species depends upon the size distribution assumed. Here, we use ~310 km of in-situ observations from flights of the South Dakota School of Mines T-28 storm penetrating aircraft to constrain the representation of the Particle Size Distribution (PSD) of hail. The maximum ~1km hail water content encountered was 9 g m^{-3}. Optical probe PSD measurements are normalized using 2-moment normalization relations to obtain an underlying exponential shape. By linking the two normalizing moments through a power-law, a parametrization of the hail PSD is provided based on the hail water content only. Preliminary numerical weather simulations indicate that the new parametrization produces increased radar reflectivity relative to commonly used PSD representations.

1. Introduction

Hail is observed on every continent but Antarctica (Cecil and Blankenship, 2012). Significant hail damage to crops and structures occurs often in regions on the flanks of mountain ranges in Europe, North America, South America, southern and eastern Africa, the European portion of Russia, and in China (Court and Griffith, 1986). Large hail is often produced by thunderstorms forming during the warm season in interior continental plains regions, such as the High Plains of the US (Changnon, 1977), the steppes of Russia (Cecil and Blankenship, 2012), and central China (Ni et al., 2016). And storm electrification is intimately tied to the growth of graupel and hail in these storms (See, e.g. MacGorman and Rust 1998, Ch. 3).

Our objective is to provide guidance on how to parameterize graupel/hail PSDs for use in cloud models. The representation of graupel (heavily rimed particles <5 mm diameter) and hail (heavily rimed particles >5 mm diameter) in models has been shown to be a source of large uncertainty in terms of cloud coverage, precipitation and cloud evolution. The 5mm size threshold for graupel to hail is from the American Meteorological Society glossary definition, but it recognized that model representations that separate graupel and hail will do so based on differing process rates or process pathways. Gilmore et al. (2004) demonstrated using idealized simulations that the precipitation amounts and condensed water species mixing ratios in deep convection were sensitive to the representation of the hail size distribution. Van den Heever and Cotton (2004) described how supercell development could be strongly modified by changing the mean size of hail particles. Similarly Cohen and McCaul (2006) noted that modifying the hail mean size affects the evaporative cooling in downdrafts that then goes on to influence the subsequent evolution of convective storms. But we note that some regional simulations have also shown less sensitivity (e.g. Van Weverberg et al. 2012). Clearly there is great uncertainty related to the representation of graupel and hail that can have an impact on the prediction and simulation of extreme weather phenomena such as large convective systems. Therefore, there is a need to constrain the representation of the particle size distribution of these species in numerical simulations of clouds and storms.

Graupel and hail particle size distributions (PSD) have been previously derived from hailpads at the surface, from aircraft using foil impactors and from optical array probes (Ulbrich and Atlas, 1982; Cheng and English 1983; Federer and Waldvogel 1975, Spahn and Smith, 1976, Morgan,1982; Smith and Jansen 1982; Peterson et al. 1991, Musil et al 1991, Heymsfield and Musil, 1982). Airborne observations have recorded hail water contents up to 3 g m^{-3} and number concentrations up to 20 m^{-3} for sizes larger than 5mm (Spahn and Smith 1976, Musil et al 1991, Heymsfield and Musil, 1982), while for hail observations at the surface lower hail water contents (<0.8 g m^{-3}, Cheng and English) and number concentrations (<4 m^{-3} for sizes>4mm) have been reported.

Aircraft based observations have indicated that hail particle sizes are distributed as a negative exponential function with increasing size when sampling is restricted to particles larger than ~5mm (Spahn and Smith, 1976). Size distribution shapes other than a simple exponential have been proposed such as a double exponential to represent different size ranges (Musil et al. 1976; Smith and Jansen, 1982), power laws (Auer and Marwitz

1972), gamma distributions (Wong et al. 1988) or truncated exponential distributions (Morgan and Summer 1975). Inclusion of sizes smaller than 5mm can include particles such as raindrops and ice aggregates that can contaminate the hail PSD. Measurements of hail PSDs at the ground can be affected by the loss of smaller hail and graupel due to melting and sublimation, or size sorting effects reducing the frequency of occurrence of smaller particles resulting in gamma- distribution-shaped PSDs (~~e.g.Jameson and Srivastava 1978,~~ (e.g. Milbrandt and Yau 2005, Kumjian and Ryzhkov 2012, and Loftus et al. 2014). In particular, Jameson and Srivastava (1978) used Doppler and radar reflectivity information to determine hail particle size distributions. They showed that below cloud base the size distributions display markedly modal distributions with a mean size of ~1.5cm while higher up (in the cloud) the hail size distributions become exponential in agreement with in-situ observations.

Graupel and hail particle densities are often represented as effective densities for a spherical particle with a diameter equal to some characteristic dimension of the actual irregular particle. Previous work, based on observed graupel and hail particles, suggests that for sizes up to 20 mm effective spherical densities (mass/volume of sphere with a diameter equal to the maximum span of the particle) can span a range from 100-910 kg m^{-3} (Magono, 1953; Braham, 1963; Bashkirova and Pershina, 1964; Zikamunda and Vali, 1972; Locatelli & Hobbs, 1974; Heymsfield, 1978; Knight and Heymsfield, 1983; List, 1985). As the particles become larger the specific density of hail derived from the immersion method of estimating density approaches that of solid ice (Prodi, 1970; Vittori and Di Caporiacco, 1959; Macklin et al., 1960). However, as hail grows larger it tends to become less spherical and so the equivalent spherical density will be lower. Recently, Heymsfield et al. (2018) combined multiple datasets using 3D laser scans of individual hailstones collected at the ground to estimate hail volume to show that the effective density of hail particles decreases with size for hail particles (5mm – 5cm).

For numerical cloud models the representation of graupel and hail density is often done by assuming a constant density. For example densities of 400 and 917 kg m^{-3} for graupel and hail respectively are assumed by Ferrier (1995). Or a power law relationship can be adopted that continuously varies the effective hydrometeor density with size (Heymsfield et al. 2018, H18: $mass[kg]=89.2D[m]^{2.69}$). Other modellers have attempted to represent the evolution of density from low values to solid ice density by predicting continuous changes to the density throughout cloud lifetime as particles become more heavily rimed (e.g. Mansell et al. 2010, Morrison and Milbrandt 2015).

Airborne hail spectrometer data has been reported previously but usually on a case study basis (e.g. Spahn and Smith 1976, Smith et al. 1976, Smith and Jansen 1982). For this study, we have synthesized hail spectrometer data from multiple flights of the South Dakota School of Mines and Technology (SDSMT) T-28 storm penetrating aircraft (Detwiler et al. 2012) to produce a normalized PSD that can be used in models that represent hail at heights close to and above the 0^{o}C temperature level. The parametrization can also be potentially used for graupel, but the 5mm lower size threshold of the observations would constitute an assumed extrapolation of these results into the size range more appropriate for graupel. We briefly test our results in a modelling framework in this study but leave the challenge of a more detailed comparison of hail in observed and simulated storms to a later paper. These normalized PSDs do not necessarily apply to observations made at the surface due to melting and evaporation experienced by hail falling below cloud base.

2. Hail spectrometer description

The SDSMT Hail Spectrometer was designed and built for use on the T-28 aircraft and is described in detail by Smith and Johnson (1980). The probe is a 1-D optical array probe, and although modified to a 2-D probe in the 1980s, the particle data was still recorded in the archive data used here as 1-D vertical size information collected along roughly horizontal aircraft tracks. The probe was mounted as two pylons under the left wing of the aircraft. A sheet of laser light emitted from one pylon illuminates a photodiode detector array behind a window in the other pylon. The detector array has 128 photodiodes with 0.9mm separation. The pylon spacing is 90cm leading to a sample volume of ~10 m^3 s^{-1}, or 100 m^3 km^{-1} for a typical 100 m s^{-1} aircraft speed. The maximum number of vertically-arrayed photodiodes occluded as a particle passes through the light sheet is taken as a measure of hail size. Although the photodiode array had a total height of 11.5 cm, size distributions are recorded only in the 5mm to 5cm range, with increasing size bin width as size increases. During missions, guidance from a meteorologist on the ground with access to data from a research-grade weather radar was provided to the pilot so that areas with hail larger than 5 cm could be avoided. Hail this large could have caused serious damage to the armored aircraft.

3. Data treatment

The data analyzed here were obtained with the hail spectrometer on a number of flights in different projects. The counts per size bin (particles that occluded the edge of the detector array were excluded) in 1-s records (Honomichl 2011, Honomichl et al. 2013) were combined with air temperature to filter out regions warmer than the 0^{o}C level. Pilot reports were used to identify the time periods where hail was encountered. Depending on pilot workload during the flight and the main objectives of the project in which the aircraft was participating, hail encounters may not have been always reported by the pilot. But if hail was reported by the pilot then it was present. A time window of +/- 1 minute was used to recover 10-s PSDs (~1km horizontal resolution for a typical 100 m s^{-1} airspeed) from that reported time, which given the probes' sample volume, would be able to detect a concentration as low as 0.01m^{-3}. Overall, this meant that we used ~310 10-s PSDs, or ~310km of along-track cloud sampling, from 18 flights over Colorado, Oklahoma and Kansas from 1995 to 2003 (see Table 1). These data were from altitudes where the air temperature was between 0 and -12^{o}C and the aircraft was flying straight and level (some profiles were not included due to potential fogging of the optical surfaces in the probe on descent to warmer lower altitudes). Surface radar information was relayed from the ground to the pilot in order to avoid flying in regions with reflectivity > 55 dBZ. Therefore, there is some sampling bias that will mean that the largest hailstones in these storms may have been avoided.

Other ways of determining when the hail was present were attempted. These included i) listening to the aircraft audio record, which included a track recorded from a microphone attached to the front windscreen, but there was too much background noise to distinguish impacts of hail; ii) inspecting imagery from a Particle Measuring Systems 2D-C optical array probe, but shape information is only robust for particles smaller than 500 microns and these size particles cannot confidently be linked to the population starting at 5mm measured by the hail spectrometer. iii) the occurrence of large particles observed with the hail spectrometer (diameter>4cm) was also considered, but this does not always correlate with when hail was reported. (These large particles might have been large snow aggregates in some cases, for instance.) Therefore, taking PSDs centered around the pilot's hail reports seem the most reliable way to capture hail PSDs. But it is accepted that these will potentially be contaminated by non-hail particles and may miss some that were not reported. If the properties of particles larger than 5mm (the minimum size of the particles detected) are different between the hail regions and non-hail regions then we should be able to observe this by changing the length of the averaging window centered around the pilot report of hail. We tested the impact of varying the length of the time window centred on the pilot report of hail to determine if the choice of +/- 60s was justified. This was done by examining the mean values of measured moments of the PSDs as a function of the window length. Because of the 5mm minimum size threshold for the observations it is expected that hail particles will have higher concentrations than other particle types in this size range. Figure 1 shows the result for the geometric mean of the concentration (other moments show the same behavior). This plot indicates that the mean concentration remains approximately constant for small time periods centred around the pilot report, but rapidly departs towards the mean of the whole dataset that includes non-hail regions as Δt exceeds 100s becoming constant again for $\Delta t > 1000$s as the non-hail regions dominate the statistics. Therefore a choice of ±60s for the window length appears acceptable. Later we will show that inspection of histograms of the PSD moments indicates that the hail population is distinct from the distributions of the whole population. For each PSD the (truncated - 5mm to 5cm) moments are calculated and used to define the fit parameters.

Additional filtering of the PSDs included removing PSDs that appeared to be contaminated by electronic noise. These PSDs were identified by filtering out anomalously flat distributions of particles counted. Visual inspection of the PSDs indicated that the 2.5-3 cm size bin sometimes reported a much higher number of counts than the neighboring two size bins. This was believed to be possibly due to electronic noise affecting a group of detectors on the probe. To alleviate this problem the particle count in this bin was replaced by the mean of the adjacent size bins. No particle-by-particles information or interarrival time data were available to assess for the effects of particle shattering, but we note that lower resolution probes are less susceptible to the effects of shattering that dominate particles sizes of a few hundred microns and smaller (e.g. Field et al. 2006).

4. Normalizing the Particle Size Distributions

Process rates involving hydrometeor species in bulk microphysics schemes used in cloud models need some assumption about the shape of the size distribution. This is commonly done by assuming a functional form and determining the parameters that define it.

We can make an assessment of the underlying shape of the PSD by normalizing the observations. To normalize the PSD, no assumption needs to be made about the final shape of the distribution (e.g. Testud et al. 2001, Lee et al. 2004, Field et al. 2007). But because the measured distribution is truncated we will assume a functional form to allow extension of the PSD to smaller and larger sizes. As we will see, an exponential distribution will be adequate to describe the data and we define it as:

$$N(D) = N_g \exp(-\lambda D) \tag{1}$$

where $N(D)\mathrm{d}D$ is the particle number concentration [m^{-3}, assuming SI units] between sizes D [m] and $D + \mathrm{d}D$. N_g [m^{-4}] and λ [m^{-1}] are the 'intercept' and 'slope' parameters that define the exponential distribution. We did a trial using a generalized gamma function but found that it did not improve the fit much and would still require assumptions about the shape parameter to carry out the exercise of adjusting for the PSD truncation described below.

Numerical weather prediction models that represent hail and/or graupel prognose the water content of this species. To be able to predict the PSD as a function of the total hail water content the mass-size relation needs to be introduced

$$m_g = \alpha D^{\beta}$$

Where m_g is the particle mass [kg]. If we assume a spherical geometry then we are assuming a constant bulk density for the hail and β would be 3. However, we make the exponent variable to allow for changing effective spherical density with size. Where effective density is the density that a sphere of the same maximum size of a non-spherical particle would possess to have the same mass as the particle.

For the normalization we define the n^{th} complete moment of the PSD as

$$M_n = \int_0^\infty D^n N(D) dD = \frac{N_g \Gamma(n+1)}{\lambda^{n+1}}, \qquad (2)$$

where Γ is the gamma function. We note that the use of the observed size distribution necessarily means that we are dealing with truncated distributions that in this case start at 5mm (D_l) and end at 5cm (D_u). Therefore we have the n^{th} truncated moment of the observed distribution as

$$m_n = \int_{D_l}^{D_u} D^n N(D) dD = \frac{N_g}{\lambda^{n+1}} \left[\gamma(n+1, \lambda D_u) - \gamma(n+1, \lambda D_l) \right], \qquad (3)$$

where γ is the incomplete gamma function.

If the characteristic size of the distribution approaches these thresholds sizes (5mm or 5cm) the measured moments will be biased relative to a distribution that extends from 0 to infinity. We also note that due to the relatively small sample size available that moment estimates are likely to be biased (e.g. Smith and Kliche, 2005). Using ratios of moments can mitigate this effect to some extent.

Two moments (integrating from 0 to infinity) can be combined to define a characteristic size for the PSD. Here we choose the β th and the $\beta + 1$st moments. This quotient gives mass weighted mean size, D_m.

$$D_m = \frac{\int \alpha D^{\beta+1} N_g \exp(-\lambda D) dD}{\int \alpha D^{\beta} N_g \exp(-\lambda D) dD} = \frac{M_{\beta+1}}{M_\beta} = \frac{\beta+1}{\lambda}, \qquad (4)$$

and rearranging gives the slope parameter,

$$\lambda = \frac{(\beta+1) M_\beta}{M_{\beta+1}}. \qquad (5)$$

We can now use the assumption about the size distribution shape and the estimate of the slope parameter to compute complete moments from the measured truncated moments. By using the initial estimate of λ derived from the measurements we can use a rearrangement of (2) and (3):

$$\mathrm{M_n} = \mathrm{m_n} \frac{\Gamma(\mathrm{n}+1)}{\gamma(\mathrm{n}+1, \lambda \mathrm{D_u}) - \gamma(\mathrm{n}+1, \lambda \mathrm{D_l})} \qquad (6)$$

to provide improved estimates of the complete moment. The new estimates of the complete moment are then used to update the estimate of λ and the process is iterated until λ values become unchanging (within 1%). An approach like this was previously used by Vivekanandan et al., 2004, for droplet distributions and Tian et al., 2010, for ice crystal size distributions.

Once we have the complete moments and the updated exponential parameters we can proceed by assuming integrals from zero to infinity. The intercept parameter for the exponential can be linked to hail water mass, W [kg m^{-3}], through the βth moment

$$W = \alpha M_\beta = \frac{\Gamma(\beta+1) \alpha N_g}{\lambda^{\beta+1}}. \qquad (7)$$

Rearranging for N_g and substituting for λ gives

$$N_g = \frac{(\beta+1)^{(\beta+1)}}{\Gamma(\beta+1)} \frac{M_\beta^{\beta+2}}{M_{\beta+1}^{(\beta+1)}}. \quad (8)$$

Finally, substituting N_g and λ into eq. 1 leads to

$$N(D)\frac{M_{\beta+1}^{\beta+1}}{M_\beta^{\beta+2}} = \frac{(\beta+1)^{\beta+1}}{\Gamma(\beta+1)} \exp(-(\beta+1)\frac{M_\beta}{M_{\beta+1}}D) \quad (9)$$

This is similar to the normalization proposed by Sekhon and Srivastava (1971) but differs in that this expression is independent of density assumptions about hail if we assume a constant bulk density . For spheres, the density information resides in α which has canceled out. If a variable bulk density ($\beta \neq 3$) is assumed then density will start to enter the normalization through the value of β. If we assume $\beta = 3$ then plotting $\frac{M_4^4}{M_3^5}N(D)$ against $\frac{M_3}{M_4}D$ should collapse the data onto an exponential distribution with intercept $\frac{256}{6}$ and slope of -4 if the data are well represented by an exponential distribution. If this collapse agrees with the predicted behavior then this supports our choice of assuming an exponential distribution as the functional form for the hail PSD.

For an exponential distribution, to predict the PSD, two moments are required that a cloud model would ideally predict to completely define the distribution. Typically a ‘double-moment microphysics scheme’ would predict number concentration and mass concentration as required. However, many models used for numerical weather prediction currently use single moment representations and only predict mass concentration. If one moment can be parameterized as a function of the other then it will be possible to predict the PSD given one moment alone (e.g. Milbrant and Yau 2005b, Thompson et al. 2008, Zhang et al. 2008, Wainwright et al 2014) which would be convenient for bulk microphysics representations that predict hail water content but not number concentration.

We can relate moments to each other by adopting an empirical power law with a and b as constants (e.g. see Testud et al. 2001)

$$\mathrm{M}_{\beta+1} = \mathrm{a}\mathrm{M}_{\beta}^{\mathrm{b}} \quad , \qquad (10)$$

which allows the PSD parameters ($\mathrm{N_g}$, λ) to be defined by the hail water content alone and its link to M_β as follows through combining (eq. 5,7)

$$\lambda = \frac{\Gamma(\beta+2)}{\Gamma(\beta+1)} \frac{\mathrm{W}^{1-\mathrm{b}}}{\mathrm{a}\,\alpha^{1-\mathrm{b}}} \qquad (11)$$

$$\mathrm{N_g} = \frac{\Gamma(\beta+2)^{\beta+1}}{\Gamma(\beta+1)^{\beta+2}} \frac{\alpha^{(\mathrm{b}-1)(\beta+1)-1}}{\mathrm{a}^{\beta+1}} \mathrm{W}^{1+(\beta+1)(1-\mathrm{b})} \qquad (12)$$

Some microphysical representations formulate N_g in terms of λ (e.g. Ferrier 1994). If we eliminate W between eqs 11 and 12 we get

$$N_g = N_{0g}\lambda^{\delta} \tag{13}$$

Where

$$N_{0g} = \left[\frac{\Gamma(\beta+1)^{b}}{\Gamma(\beta+2)} a \right]^{\frac{1}{1-b}} \tag{14}$$

And

$$\delta = \frac{1+(\beta+1)(1-b)}{(1-b)} \tag{15}$$

5. Results

Size distributions from the hail periods (~310 10-s periods, equivalent to ~310km of sampling) are shown in Figure 2. The sizes cover the range from 5mm to 5cm; a range of sizes large snowflakes as well as hail can attain, potentially leading to overlap between the populations. Overplotted are mean PSDs for 0.01, 0.1, 1.0 and 10 g m^{-3} hail water contents (using Heymsfield et al. 2018: H18 mass[kg]=89.2D[m]$^{2.69}$). This indicates a tendency for the PSD to become broader as the intercept parameter increases.

Normalized histograms of moments of the PSD show a distinct difference between the PSDs dominated by the hail population and when all 10-sec PSDs from the set of flights are considered (Fig. 3). All of the moments for the hail population exhibit higher modal values than for the background population indicating higher water content and number concentrations for particles with size >5mm. Figure 3e uses the H18 relation to estimate the hail water contents that reach a maximum of 9 g m^{-3} for 1 10s period (approximately 1 km distance) and exhibit a mode in the observations ~0.1 g m^{-3}. Characteristic size is the mass weighted mean size assuming a mass-size exponent of 2.69. This histogram (Fig. 3f) indicates that the maximum mass weighted mean sizes encountered reaches ~3cm, while the mean is ~1cm.

Values from the literature for N_g and λ have been presented in Fig. 4a to provide some comparison to the observations. Using the 310 PSD moments, the values for N_g and λ for each PSD have been calculated and plotted in Fig. 4b . For this study N_g and λ have ranges of $2x10^1$ - $3x10^4$ m^{-4} and 100-900 m^{-1}, respectively. The range of values for this study is in agreement with previous work and towards the lower λ end (i.e. broader distribution) of the range of reported values. Also shown in Figure 4a are some examples of intercept parameter used in cloud microphysical representations of graupel and hail. These intercept values used in the models tend to be above the observed range reported here. For the same water content this would mean that the model particle mean sizes would be smaller, their fallspeed slower and so increase the residence time of the hail within the cloud.

The hail PSDs have been normalized using the 3rd and 4th moment and plotted in Figure 5a. The collapse of the data reduces the spread from 2.5 orders of magnitude (Fig. 2) to about 1 order of magnitude. The normalized distribution is approximated quite well by an exponential distribution (the expected exponential curve for a 3^{rd} and 4^{th} moment normalisation is overplotted: intercept=256/6, slope=-4), supporting our choice of an exponential distribution to represent the PSD.

Finally, cloud microphysical representations that use a single moment, such as the hail water content to represent hail, need to parameterize one of the moments in terms of the moment prognosed by the model. Figure 5b shows power law relationships between the β and $\beta + 1$ moments where here β=3, 2.69. It can be seen that the power laws vary slightly in terms of the exponent. The best fit lines to relate the moments shown in figure 5b are

$$M_4 = 0.10 M_3^{1.15} \quad (16)$$

$$M_{3.69} = 0.10 M_{2.69}^{1.19} \quad (17)$$

Table 2 uses the power law relation for the moments to generate the parameters required for estimating the PSD based on hail water content only from eqs 11, 12.

The results indicate that as water content increases, N_g increases and λ decreases as was seen in figure 2. This decrease in λ with increasing water content is similar to behavior reported by Knight et al. (1982) in the US National Hail Research Experiment (conducted in 1972-1976) for increasing precipitation rate based on data from the hail spectrometer and a foil impactor on the SDSMT armored T-28. This means that the intercept parameter (or concentration) increases at the same time as the distribution gets broader (or mass weighted mean particle size gets larger).

Figure 4b includes two results for the single moment parameterization, using equation 13 with values given in table 2 overplotted, as curves. The grey curve uses a constant bulk density to relate size to mass, while the black curve is based on the mass-size relationship from H18. In principle a double moment representation of hail would be able to better cover this phase space. But because the hail PSD representation has been reduced to a single moment, it is not able to cover all of the phase space that the observed size distributions explore, and instead follows a trajectory that bisects the data. Microphysics process rates or diagnostics ultimately use different moments of the size distribution. For a parametrization of the PSD based on the mass moment that is close to 3 the least well predicted moments of interest are expected to be the number concentration (0^{th}) and the radar reflectivity (6^{th}). Figure 6 shows the predicted and measured (adjusted to represent a PSD extending from zero to infinity in particle size as described above) 0^{th}, 6^{th} moments and the exponential distribution parameters (λ, Ng). The geometric means and standard deviations suggest that, over the range of the data used, the mean predicted values are a factor of 1.4 and 0.6 of the measured values for M_0 and M_6, respectively. Geometric standard deviations indicate that the variability is a factor of 3 around the mean value. Similarly the parametrized values of λ and N_g based on water content (table 2) can be compared to those derived from the PSDs and the mean bias and standard deviation can be assessed of the ratio of parametrized to observed. It was found that for λ-parametrized/λ-observed the mean and standard deviation was 1.2 and 0.5. And for $\log_{10}(N_g\text{-parametrized}/N_g\text{-observed})$ the mean and standard deviation was 0.2 and 0.6. The parametrized N_g is more biased than the parametrized λ because it is more related to number concentration than the mass defined reference moment used in the analysis. A parametrization using the concentration could be constructed to reduce the bias in N_g, but because the moments of the process rates that are important (sedimentation, collection) are closer to the moment linked to the water content (~3) it would be less useful for modelling.

6. Model testing

We have used the Met Office Unified Model to test the impact of changing the rimed particle PSD relationship. The model uses a single mass only representation of graupel based on a gamma distribution: $N(D)=N_g D^{\mu} exp(-\lambda D)$, where N_g is given by equation 13. In the operational model the values are: N_{0g}=5e25, δ=-4.0, μ=2.5 ('Control') and an effective density of 500kg m^{-3} is assumed. For the test we take the values for the same density in table 2: ('This study') N_{0g}=7.9e9, δ=-2.58, μ=0 (where μ=0 comes from the assumption of an exponential distribution) and the values for a more widely used assumption based on Lin et al. (1983): N_{0g}=4e4, δ=0.0, μ=0 ('Lin'), for comparison. Strictly, the PSD observations and parametrization is for hail particles between 5mm and 5cm in size. However, we have applied the PSD to all rimed particles represented in the model. We note that radar reflectivity is derived directly from the hail size distribution ($Ze \sim D^6$) parameters assuming a constant density of 500 kg m^{-3}, assuring consistency between the microphysical treatment of the hail and the radar response.

The case study is from the 20th May 2013, where an EF5 tornado caused significant damage in and around the city of Moore, Oklahoma. The model configuration is as described in Stratton et al (2018), but with a finer horizontal grid resolution of 1.5 km and 70 vertical levels with stretched vertical spacing (~100m at 1km). The domain of the simulation is as shown in figure 7. The model is initialized at 00Z on 20 May 2013 and run for 24 hours. Model fields are inspected and compared for T+20 (to coincide with the reported timing of the tornado on the ground). Here we will comment on the qualitative differences in simulated reflectivity patterns due to changing the PSD alone and leave the challenge of verification with data for a later paper. The ability to reproduce observed radar reflectivities is a challenging problem. It relies on the accurate representation of not only the hail/graupel particle size distribution but also 1) the microphysical process rates that provide sources and sinks for graupel/hail, that are highly uncertain; 2) the radar forward model to convert the model PSD into reflectivity and the radar wavelength assumed; 3) accurate reflectivities from the other condensed water species that will contribute to the radar response and impact the sources and sinks of graupel/hail. The points 1,2 and 3 will be different for different numerical weather models. Our approach here is to demonstrate the relative response of the model using the new PSD relative to using a classic one from the literature to provide motivation for others to assess the impact of this PSD in their model. This work provides an in situ based observational constraint around which more uncertain aspects such as microphysical hail source (e.g. riming and droplet freezing) and sink rates (e.g. melting and shedding) can be tuned.

From figure 4 it is clear that the diagnosed concentrations will be lower in the parametrization proposed in this study than is ordinarily used. This will mean that for the same water mass there will be lower concentrations of particles but the mean size and hence mean fallspeed will be larger. Therefore, for larger particles we would expect that, all things being equal, we will see reduced hail water paths and potentially increased radar reflectivity signals (if not offset by reduced water mass). Figure 7 shows the result of the test compared to the UM control PSD representation and the widely used Lin et al. (1983) PSD representation. The control and Lin PSD produce similar results in terms of composite reflectivity, hail water path and a lack of hail seen at the surface. For the new PSD presented in this work, it can be seen that the radar composite reflectivity (maximum reflectivity in the vertical column) increases, while the hail water path decreases. The new PSD is the only representation that indicates hail at the surface with max hail sizes of up to 25 mm.

7. Conclusions

Using a comprehensive hail data set collected in-situ at temperatures 0^{0}C and below with an airborne instrument that has large sample volumes relative to data collected at the ground, normalization of the PSD using moments of the distribution indicates that the hail PSD can be represented as an exponential between diameters of 5 mm and 5 cm. Hail water contents of up 9 g m^{-3} (in 10 s or 1km of flight sample) were inferred. Exponential distribution intercept parameters derived from these results suggest that commonly used exponential intercept values for models are larger than observed in-cloud. By linking two moments of the size distribution together with a power law, the parameters of the exponential distribution are predictable from hail water content alone. However, the variability exhibited by the intercept parameters suggests that the ability to predict two moments of the hail distribution may be advantageous for modelling the evolution of hail. The results of our study have considerable utility for modeling the development of graupel and hail within convection. A preliminary test of the new PSD parametrization indicates that radar reflectivities are increased, and more hail is able to survive to fall to the surface at warmer temperatures, relative to simulations with a previous more commonly used PSD representation.

Acknowledgments

Thanks to Shawn Honomichl who provided the 1-s PSD data from the T-28 hail spectrometer. Thanks to Paul Smith for comments on an earlier version of the manuscript.

NCAR affiliate scientist program paid for PF to work with AH and AD on analyzing data and preparing the manuscript. AH is supported by the National Science Foundation.

References

Auer A.H, and J. D. Marwitz, 1972. Hail in the vicinity of organized updrafts. Journal of Applied Meteorology, 11, 748-752.

Bashkirova, G.M. and T.A. Pershina. 1964. O masse snezhinok iskorosti ikh padeniya [On the mass of snow crystals and their fall velocity]. Transactions of the Main Geophysical Observatory, 165, 83–101.

Braham, R.R., 1963: Some measurements of snow pellet bulk-densities. Journal of Applied Meteorology, 2, 498–500.

Changnon, S. A., Jr., 1977: The climatology of hail in North America. In Hail: A Review of Hail. Science and Hail Suppression. Meteor. Monogr., 38, G. B. Foote and C.A. Knight, Eds.,. Amer. Meteor. Soc., Boston, Mass., 107-128

Court A., and Griffiths J.F. 1986: Thunderstorm climatology. In 'Thunderstorm morphology and dynamics' Ed Kessler E., University of Oklahoma Press. D00A18, doi:10.1029/2008JD009982.

Cheng, L., M. English, and R. Wong1985: Hailstone size distributions and their relationship to storm thermodynamics. Journal of Climate and Applied Met., 24, 1059–1067.

Cecil, D.J. and C.B. Blankenship, 2012: Toward a Global Climatology of Severe Hailstorms as Estimated by Satellite Passive Microwave Imagers. J. Climate, 25, 687–703,

Cohen, C. and E.W. McCaul, 2006: The Sensitivity of Simulated Convective Storms to Variations in Prescribed Single-Moment Microphysics Parameters that Describe Particle Distributions, Sizes, and Numbers. Mon. Wea. Rev., 134, 2547–2565.

Detwiler, A., J. Scannell, D. Kliche,, and S. Williams, 2012: Creating the long-term T-28 instrumented research aircraft data archive. Bulletin of the American Meteorological Society, **93**, 1817–1820, https://doi.org/10.1175/BAMS-D-11-00066.1

Federer, B. and A. Waldvogel,1975: Hail and raindrop size distributions from a Swiss multicell storm. Journal of Applied Meteorology, 14, 91–97.

Ferrier, B., 1994: A Double-Moment Multiple-Phase Four-Class Bulk Ice Scheme. Part I: Description. J. Atmos. Sci., 51, 249–280

Field, P.R., A. J. Heymsfield, and A. Bansemer, 2006: Shattering and particle interarrival times measured by optical array probes in ice clouds. J. Atmos. Oceanic Technol. 23, 1357-1371.

Field, P.R., A. J. Heymsfield, and A. Bansemer, 2007: Snow size distribution parameterization for midlatitude and tropical ice clouds. Journal of Atmospheric Sciences, **64**, 4346–4365

Fraile, R., J. L. Sanchez, J., J. L. de la Madrid, et al.1999. Some results from the hailpad network in Leon (Spain): Noteworthy correlations among hailfall parameters. Theoretical and Applied Climatology, 64 (1-2): 105-117.

Gilmore, M.S., J.M. Straka, and E.N. Rasmussen, 2004: Precipitation and Evolution Sensitivity in Simulated Deep Convective Storms: Comparisons between Liquid-Only and Simple Ice and Liquid Phase Microphysics. Mon. Wea. Rev., 132, 1897–1916.

Heymsfield, A.J., 1978. The characteristics of graupel particles in northeastern Colorado cumulus congestus clouds. Journal of Atmospheric Sciences, 35, 284-295.

Heymsfield, A.J. and D. J. Musil, 1982: Case study of a hailstorm in Colorado. Part II: Particle growth processes at mid-levels deduced from in-situ measurements. Journal of Atmospheric Sciences, **39**, 2847–2866.

Heymsfield A. J., M. Szakáll, A. Jost, I. Giammanco and R. Wright, 2018: A Comprehensive Observational Study of Graupel and Hail Terminal Velocity, Mass Flux and Kinetic Energy. Submitted to J. Atmos. Sci.

Hong S-Y and J-O J. Lim, 2006: The WRF single-moment 6-class microphysics scheme (WSM6). Journal of the Korean Meteorological Society, 42, 2, 129-151.

Honomichl S.B. 2011. Climatologies of convective flight environments for use in the development of a storm penetrating aircraft. Master of Science thesis held by South Dakota School of Mines.

Honomichl S.B., A. G. Detwiler, and P. L. Smith, 2013: Observed hazards to aircraft in deep summertime convective clouds from 4–7 km", Journal of Aircraft, 50(3), pp. 926-935.

Jameson, A.R. and R.C. Srivastava, 1978: Dual-Wavelength Doppler Radar Observations of Hail at Vertical Incidence. J. Appl. Meteor., 17, 1694–1703.

Knight, N. C. and A. J. Heymsfield, 1983. Measurement and interpretation of hailstone density and terminal velocity. Journal of Atmospheric Sciences 40 (6): 1510-1516.

Knight , C. A., W. A. Cooper, D. W. Breed, I. R. Paluch, P. L. Smith and G. Vali, 1982: Chapter 7. Microphysics. In Hailstorms of the Central High Plains, Vol 1:The National Hail Research Experiment. , C. A. Knight and P. Squires, eds. Colorado Associated University Press, Boulder, Colorado. pp. 151-193.

Kumjian, M.R. and A.V. Ryzhkov, 2012: The Impact of Size Sorting on the Polarimetric Radar Variables. J. Atmos. Sci., 69, 2042–2060.

Lee, G., I. Zawadzki,, W. Szyrmer, D. Sempere-Torres and R. Uijlenhoet, 2004: A general approach to double-moment normalization of drop size distributions. Journal of Applied Meteorology, **43,** 264–281.

Lin, Y.L., R. D. Farley, H. D. Orville, 1983: Bulk parameterization of the snow field in a cloud model. Journal of Applied Meteorology, 22, 1065–1092.

List R. 1985: Properties and growth of hailstones. In ‘Thunderstorms: a social, scientific and technological documentary. Vol 2. Thunderstorm morphology and dynamics.’ 2nd edition. Edited by E. Kessler, University of Oklahoma Press.

Locatelli, J. D. and P. V. Hobbs,1974. Fall speeds and masses of solid precipitation particles." Journal of Geophysical Research, 79, 2185-2197.

Loftus, A. M., W. R. Cotton, and G. G. Carrió, 2014: A triple-moment hail bulk microphysics scheme. Part I: Description and initial evaluation. Atmos. Res., 149, 35–57.

MacGorman, D. R., & W. D. Rust, 1998. The Electrical Nature of Storms. Oxford University Press, Oxford, UK. 422 pp.

Macklin W.C., E. Strauch and F. H. Ludlam, 1960: The density of hailstones collected from a summer storm. Nubila, 3,12-17.

Magono, C., 1953. On the growth of snowflakes and graupel. Science Report. Yokohama National University, Japan, Ser. I, No. 2, 18–40

Mansell, E.R., C.L. Ziegler, and E.C. Bruning, 2010: Simulated Electrification of a Small Thunderstorm with Two-Moment Bulk Microphysics. J. Atmos. Sci., 67, 171–194

Milbrandt, J.A. and M.K. Yau, 2005: A Multimoment Bulk Microphysics Parameterization. Part I: Analysis of the Role of the Spectral Shape Parameter. J. Atmos. Sci., 62, 3051–3064.

Morrison, H. and J. A. Milbrandt,, 2015: Parameterization of cloud microphysics based on the prediction of bulk ice particle properties. Part I: Scheme description and idealized tests. J. Atmos. Sci., 72(1), 287-311.

Musil D. J., S. A. Christopher, R. A. Deola, and P. L.Smith, 1991. Some interior observations of southeastern Montana hailstorms. Journal of Applied Meteorology, 30, 1596-1612.

Ni, X., C. Liu, Q. Zhang, and D. J. Cecil (2016), Properties of hail storms over China and the United States from the Tropical Rainfall Measuring Mission, J. Geophys. Res. Atmos., 121, 12,031–12,044, doi:10.1002/2016JD025600.

Peterson, B. A., D. J. Musil, and P. L. Smith, 1991: Computerized reduction of airborne foil impactor data. Journal of Atmospheric and Oceanic Technology, 8, 691-696

Prodi, F., 1970: Measurements of local density in artificial and natural hailstones. Journal of Applied Meteorology,9,903–910.

Sekhon, R.S. and R. C. Srivastava. 1971: Doppler radar observations of drop-size distributions in a thunderstorm. Journal of Atmospheric Sciences, 28, 983-994.

Spahn J.F. and P. L. Smith, 1976. Some Characteristics of Hailstone Size Distributions Inside Hailstorms. Preprint Volume: 17th Conference on Radar Meteorology. Oct 26-29, 1976, Seattle, Washington. American Meteorological Society.

Smith, P. L., Jr., D. J. Musil, S. F. Weber, J. F. Spahn, G. N. Johnson, and W. R. Sand, 1976: Raindrop and hailstone size distributions inside hailstorms. Preprints, International Conference on Clouds Physics, Boulder, Colorado ,252-257

Smith, P.L. and D. C. Jansen,1982: Observations inside SESAME thunderstorms with an airborne hail spectrometer. 12th Conference on Severe Local Storms. San Antonio, Texas, 16-19. American Meteorological Society

Smith, P.L. and D. V. Kliche,2005: The bias in moment estimators for parameters of drop size distribution functions: Sampling from exponential distributions. Journal of Applied Meteorology, 44, 1195–1205, https://doi.org/10.1175/JAM2258.1

Stratton, R. A. and coauthors, 2018: A Pan-African Convection-Permitting Regional Climate Simulation with the Met Office Unified Model: CP4-Africa. Journal of Climate, 31, 3485–3508, https://doi.org/10.1175/JCLI-D-17-0503.1

Testud, J., S. Oury, R. A. Black, P. Amayenc. and X. K. Dou, 2001: The concept of "normalized" distribution to describe raindrop spectra: A tool for cloud physics and cloud remote sensing. Journal of Applied Meteorology., **40,** 1118–1140.

Thompson, G., P. R. Field, R. M. Rasmussen, and W. D. Hall, 2008: Explicit forecasts of winter precipitation using an improved bulk microphysics scheme. Part II: implementation of a new snow parameterization. Monthly Weather Review, **136**, 5095–5115.

Tian, L., G.M. Heymsfield, L. Li, A.J. Heymsfield, A. Bansemer, C.H. Twohy, and R.C. Srivastava, 2010: A Study of Cirrus Ice Particle Size Distribution Using TC4 Observations. J. Atmos. Sci., **67**, 195–216

Ulbrich, C.W., and D. Atlas,1982: Hail parameter relations: A comprehensive digest. Journal of Applied Meteorology, 21, 22–43.

Van den Heever, S.C. and W.R. Cotton, 2004: The Impact of Hail Size on Simulated Supercell Storms. J. Atmos. Sci., 61, 1596–1609.

Van Weverberg, K., A.M. Vogelmann, H. Morrison, and J.A. Milbrandt, 2012: Sensitivity of Idealized Squall-Line Simulations to the Level of Complexity Used in Two-Moment Bulk Microphysics Schemes. Mon. Wea. Rev., 140, 1883–1907

Wong, R.K., N. Chidambaram, L. Cheng, and M. English 1988: The sampling variations of hailstone size distributions. Journal of Applied Meteorology, **27**, 254–260.

Vittori O. and G. Di Caporiacco, 1959: The density of hailstones. Nubila, 2, 51-57.

Vivekanandan, J., G. Zhang, and E. Brandes, 2004: Polarimetric Radar Estimators Based on a Constrained Gamma Drop Size Distribution Model. J. Appl. Meteor., 43, 217–230

Wainwright, C.E., D.T. Dawson, M. Xue, and G. Zhang, 2014: Diagnosing the Intercept Parameters of the Exponential Drop Size Distributions in a Single-Moment Microphysics Scheme and Impact on Supercell Storm Simulations. J. Appl. Meteor. Climatol., 53, 2072–2090

Zhang G. M., Xue, Q. Cao, and D. Dawson, 2008: Diagnosing the intercept parameter for exponential raindrop size distribution based on video disdrometer observations: Model development. J. Appl. Meteor. Climatol., 47, 2983–2992.

Zikmunda, J., and G. Vali, G.,1972: Fall patterns and fall velocities of rimed ice crystals. Journal of the Atmospheric Sciences, 29, 1334–1347.

Tables

Table 1. List of T-28 campaigns and flights used in analysis. Flight numbers increment serially from flight to flight, beginning in 1972. For more details see: https://www.eol.ucar.edu/projects/t28/projects/

Project name/date	Flights used	Location airport
CHILL 21 July - 3 August 2003	815,819,820	Greely, Colorado
JPOLE/TELEX 15 March - 15 June 2003	798,803	Norman, Oklahoma
CHILL-TEX 3-18 June 2002	781	Greely, Colorado
STEPS May - July 2000	754,756,757,759, 761	Goodland, Kansas
TCAD June 1999	728.729,735	Ft. Collins, Colorado
VORTEX April-June 1995	658,667,668,670	Ft Collins, Colorado/Norman, Oklahoma

Table 2. Results for different geometry assumptions. All units are SI.

geometry	α	β	a	b	λ	N_g	$N_0 g$	δ
$\rho = 500$ kg m^{-3}	262	3	0.1	1.15	$98W^{-0.15}$	$57770W^{0.39}$	7.9e9	-2.58
$\rho = 910$ kg m^{-3}	473	3	0.1	1.15	$107W^{-0.15}$	$45820W^{0.39}$	7.9e9	-2.58
H18	89.2	2.69	0.082	1.14	$85W^{-0.19}$	$36570W^{0.30}$	4.7e7	-1.61

Figures

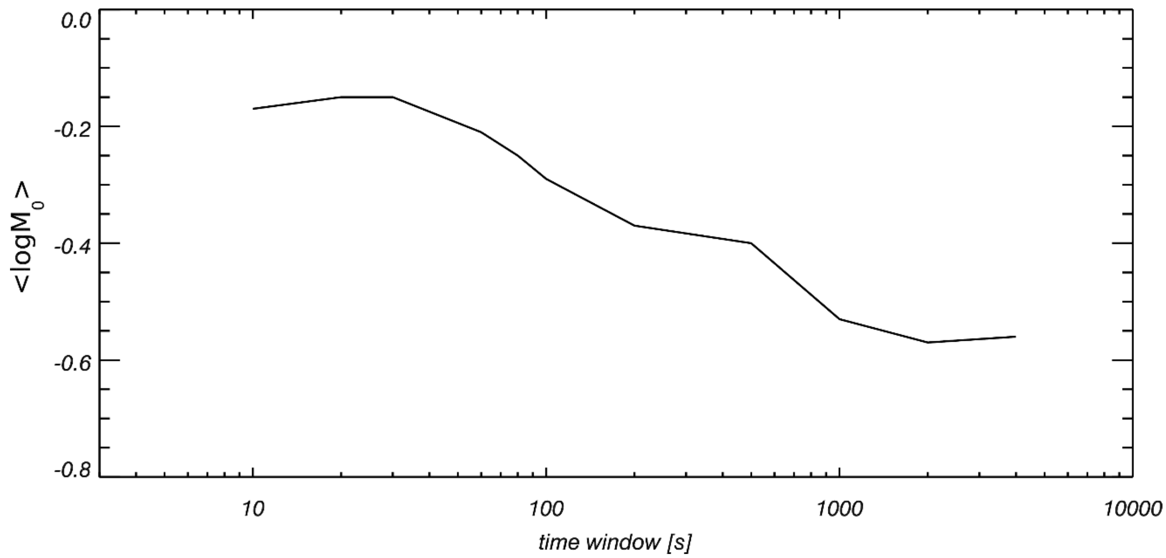

Figure 1. Mean of $\log_{10}M_0$ as a function of length of time window centred on pilot hail report.

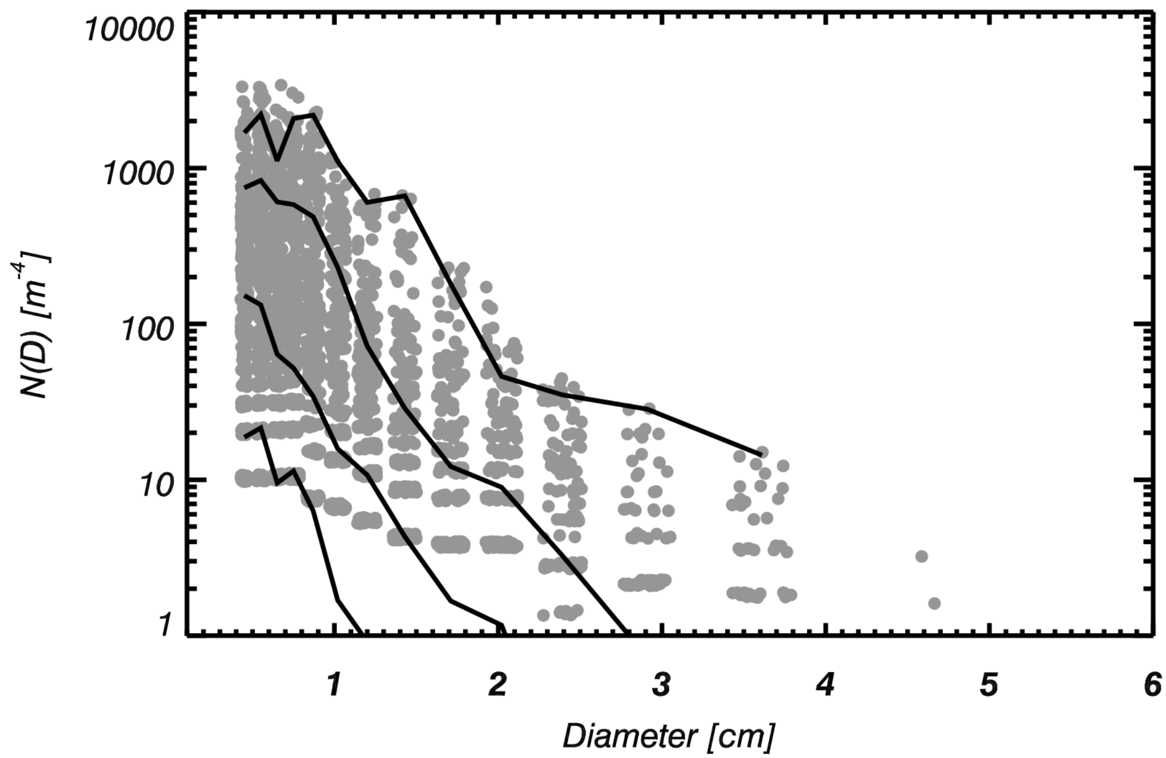

Figure 2. Particle size distributions, each computed using 10-s of data (100 m^3, 1km distance). All the data from the regions associated with pilot reports (+- 60s) of hail are shown as gray circles (310 10-s periods). Slight offset of the plotted data along the size axis is shown for clarity. Overplotted as solid lines are mean PSDs for hail water contents of 0.01, 0.1, 1 and 10 g m^{-3} from bottom to top.

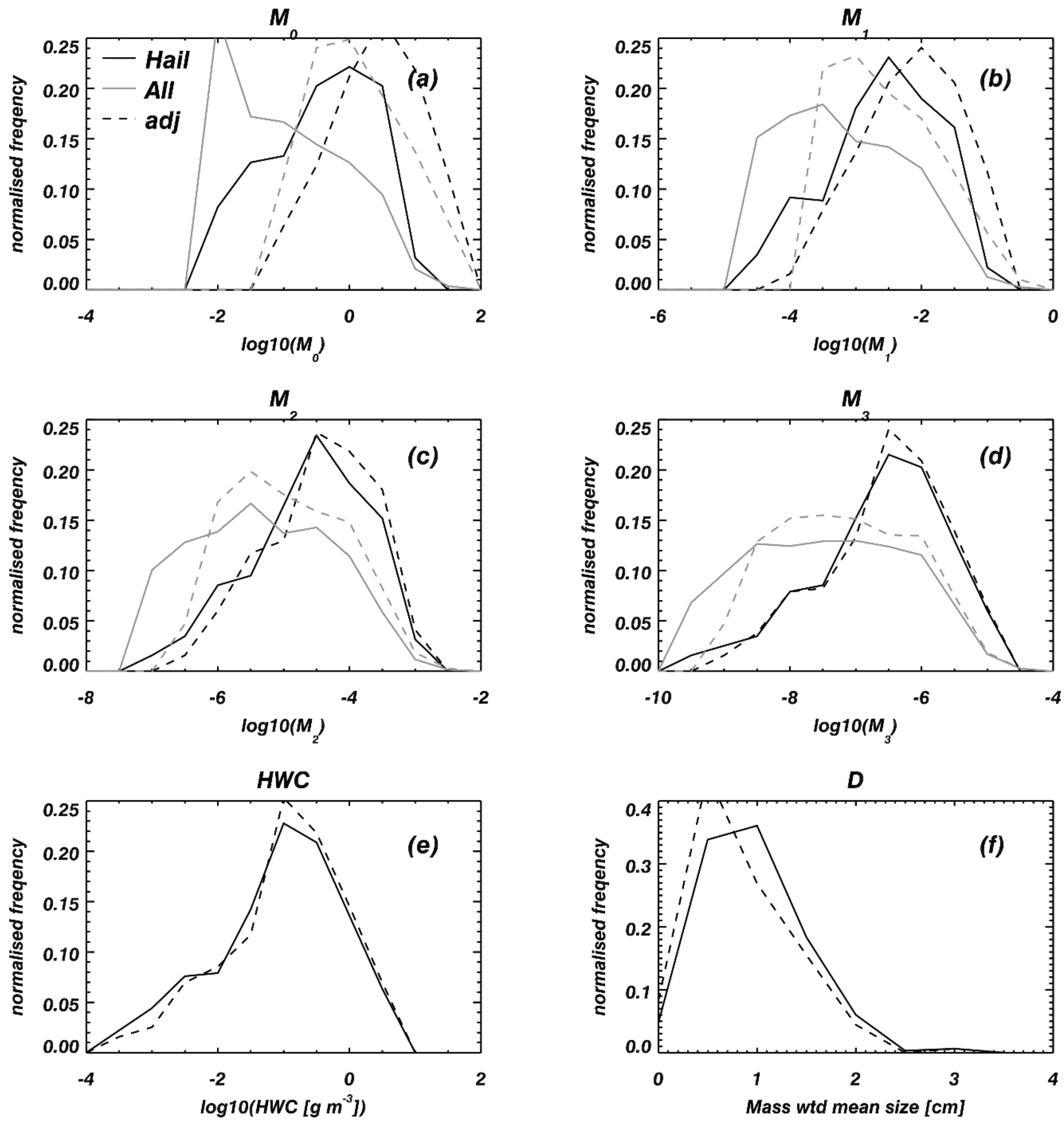

Figure 3. Normalized histograms of different moments of the PSD demonstrating that the population chosen to represent the hail is different from the overall population. (a) –(d) shows the zeroth, first, second and third moments of the size distribution. (e) hail water content. (f) is the mass weighted mean size of the distribution. Solid lines show the original measured moment and the dashed lines are the adjusted moment assuming an exponential distribution integrated from 0 to infinity.

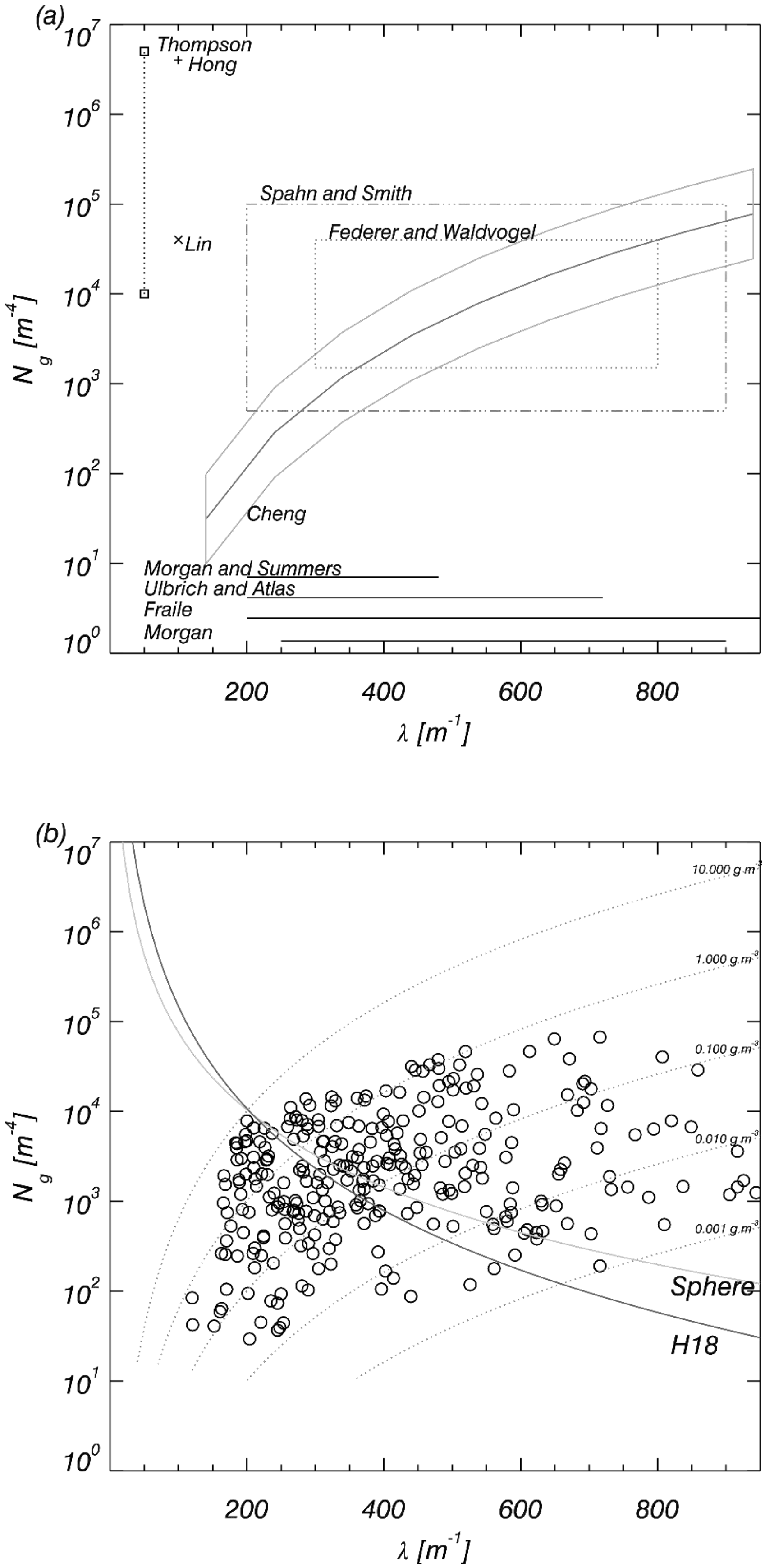

(a)
Thompson
Hong
Lin
Spahn and Smith
Federer and Waldvogel
Cheng
Morgan and Summers
Ulbrich and Atlas
Fraile
Morgan
N_g [m^-4]
λ [m^-1]
(b)
10.000 g.m^-3
1.000 g.m^-3
0.100 g.m^-3
0.010 g.m^-3
0.001 g.m^-3
Sphere
H18
N_g [m^-4]
λ [m^-1]

Figure 4. a) Previous slope and intercept parameters for exponential fits to the PSDs. The boxes (solid: Cheng et al., 1985, also shown is their N_g-λ relationship; dotted: Federer and Waldvogel. 1975; dot-dashed: Smith and Spahn, 1976) show ranges from the literature where slope and intercept were given. The horizontal lines towards the bottom of the panel show the range of slope values from the literature where only the slope was known (usually derived from hailpads). The symbols to the left of the figure indicate intercept values used for microphysics schemes in cloud models. The open squares denote the range used in Thompson et al. 2008. The '+' is from Hong et al. and the 'x' from Lin et al. b) The open circles are the slope and intercept parameters for the hail PSDs in this study. The grey solid curve, marked 'Sphere', represents the λ and N_g values assuming a constant bulk density (it is insensitive to density, but different densities will sit at a different point along the line for the same water content). The black solid curve uses the H18 mass-size relationship. The dotted lines show contours of constant hail water content based on the 500kg m^{-3} sphere density.

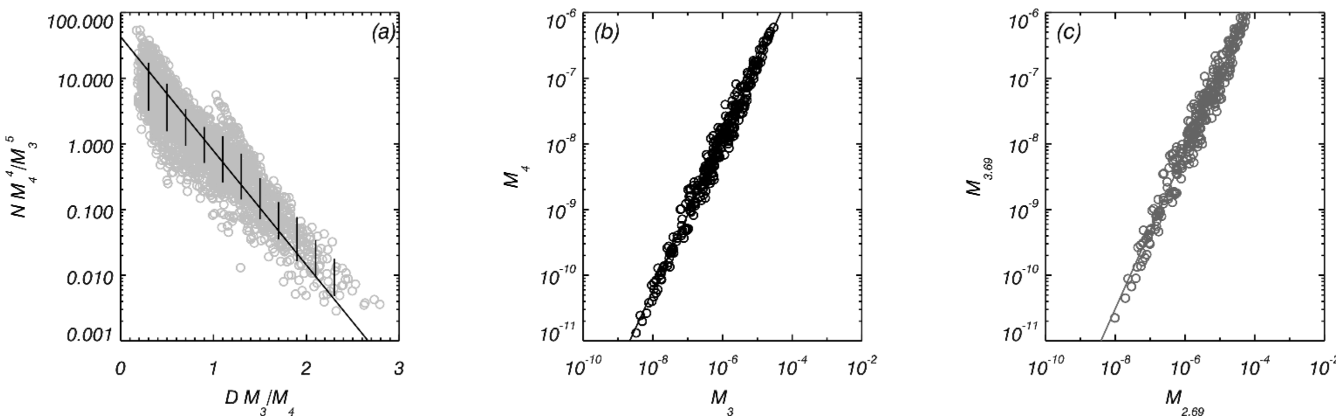

Figure 5. a) normalized size distribution using moments 3 and 4 for the hail PSDs. The solid line indicates the theoretically expected curve for an exponential distribution normalized with the 3rd and 4th moment. The variability bars indicate 1 standard deviation in log space (correlation coefficient r=-0.87). b) Power law relations between moments 3 and 4. c) the same as b) but for moments 2.69 and 3.69. The relationship between M3:M4 and M2.69:M3.69 are shown (correlation coefficients of 0.99,0.98, respectively).

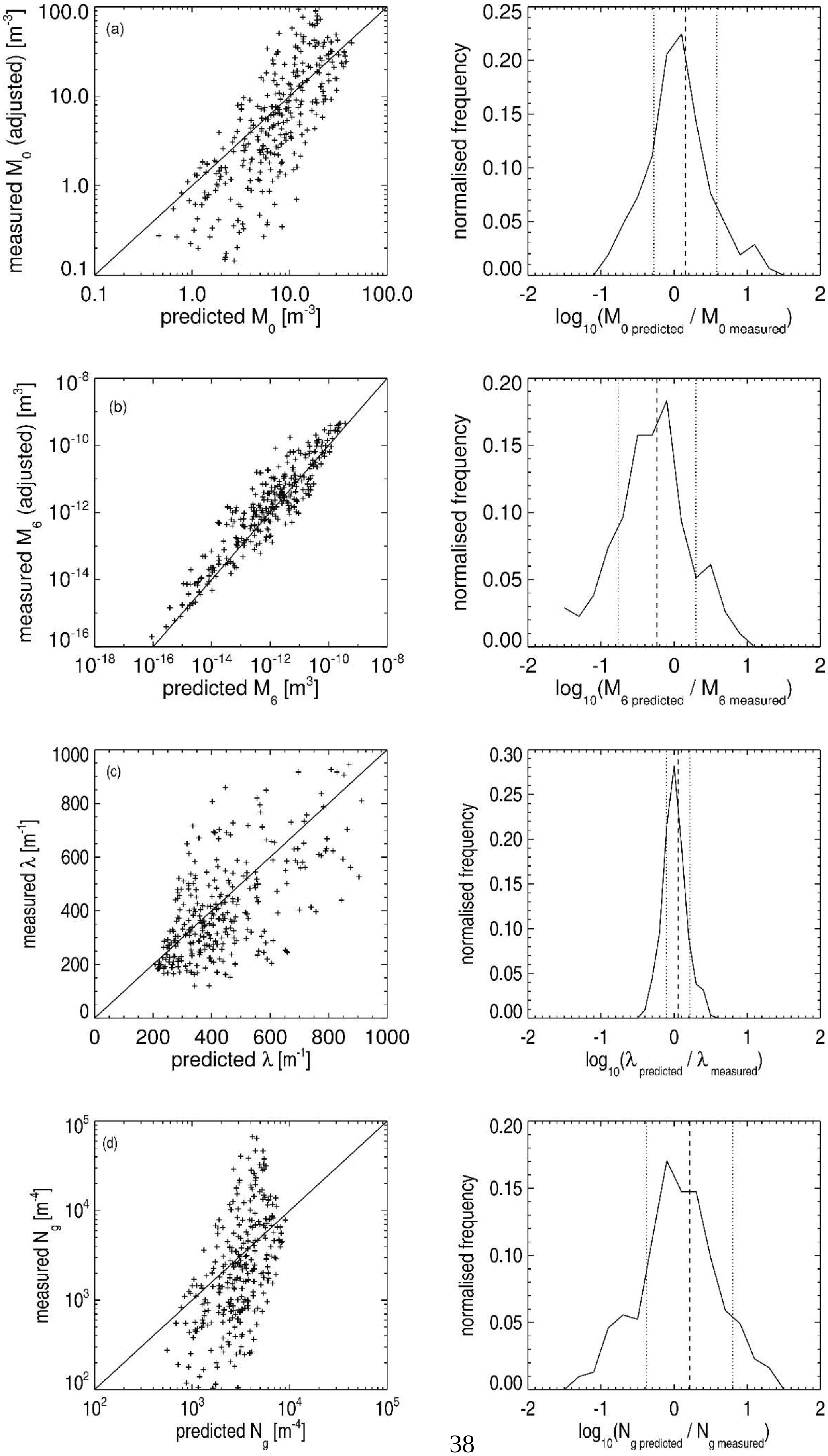
(a)
measured M0 (adjusted) [m-3]
predicted M0 [m-3]
normalised frequency
log10(M0 predicted / M0 measured)
(b)
measured M6 (adjusted) [m3]
predicted M6 [m3]
normalised frequency
log10(M6 predicted / M6 measured)
(c)
measured λ [m-1]
predicted λ [m-1]
normalised frequency
log10(λpredicted / λmeasured)
(d)
measured Ng [m-4]
predicted Ng [m-4]
normalised frequency
log10(Ng predicted / Ng measured)

Figure 6. a) predicted complete zeroth moment versus measured adjusted zeroth moment (i.e. concentration). Correlation coefficient r=0.79. b) Same as a) but for 6^{th} moment. Correlation coefficient r=0.94. c) predicted and measured λ, correlation coefficient r=0.72 d) predicted and measured $N_{g,}$, correlation coefficient r=0.57 The 1:1 lines are overplotted for all panels. Right panels show histograms of the logarithm of the ratio of the predicted to measured parameters depicted in the left panels. The geometric mean is

shown as a vertical dashed line with 1 geometric standard deviation either side of the mean shown as dotted lines.

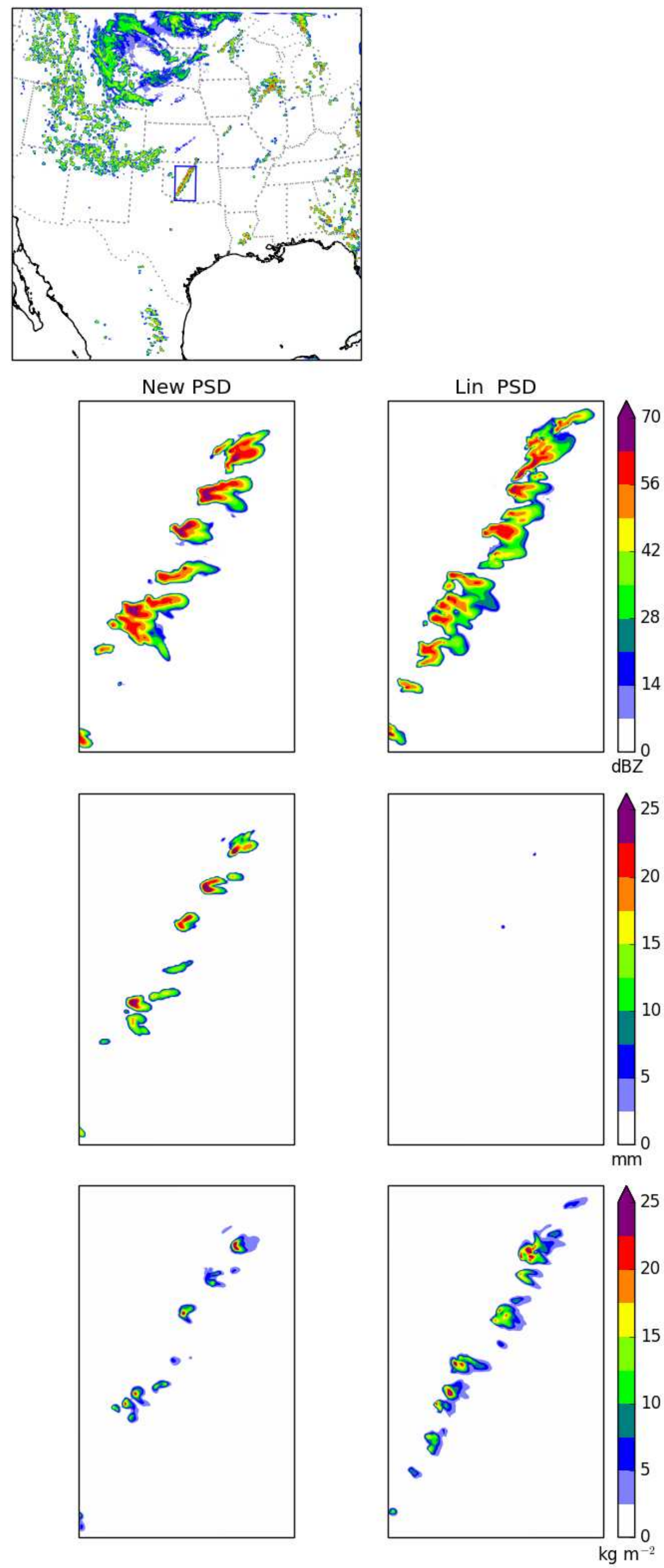
Control
New PSD
Lin PSD
70
56
42
28
14
0
dBZ
25
20
15
10
5
0
mm
25
20
15
10
5
0
kg m⁻²

Figure 7. Top panel – location map: blue rectangle is region of interest. Model sensitivity tests for 20 UTC 20 May 2013 for PSD settings used for Control (left column), this study (centre column) and Lin et al. (right column). Top row: composite radar reflectivity, middle row: max hail size at surface, bottom row: hail water path.